2015 IEEE 54th Annual Conference on Decision and Control (CDC)
December 15-18, 2015. Osaka, Japan

Orthotic Body-Weight Support Through Underactuated Potential Energy Shaping with Contact Constraints

Ge Lv, *Student Member, IEEE,* and Robert D. Gregg, *Member, IEEE*

***Abstract*— Body-weight support is an effective clinical tool for gait rehabilitation after neurological impairment. Body-weight supported training systems have been developed to help patients regain mobility and confidence during walking, but conventional systems constrain the patient's treatment in clinical environments. We propose that this challenge could be addressed by virtually providing patients with body-weight support through the actuators of a powered orthosis (or exoskeleton) utilizing potential energy shaping control. However, the changing contact conditions and degrees of underactuation encountered during human walking present significant challenges to consistently matching a desired potential energy for the human in closed loop. We therefore introduce a generalized matching condition for shaping Lagrangian systems with holonomic contact constraints. By satisfying this matching condition for four phases of gait, we derive control laws to achieve virtual body-weight support through a powered knee-ankle orthosis. We demonstrate beneficial effects of virtual body-weight support in simulations of a human-like biped model, indicating the potential clinical value of this proposed control approach.**

I. Introduction

Individuals who have sustained a stroke, spinal cord injury, or other neurological condition often struggle to ambulate. Gait training is needed to help these patients regain mobility and independence. Patients are often provided with body-weight support (BWS) during training to help them produce the coordinated muscle activities needed for walking. This locomotor retraining technique provides weight support for patients through a torso or hip harnesses attached to an overhead lift [1]. The percentage of BWS is often adjusted progressively as the patient's gait improves through the training process. Over the past two decades, the use of BWS training systems to enhance ambulation and motor function in individuals has received considerable attention [2].

Current body-weight supported training systems can be classified into two categories: treadmill/stationary training systems and ceiling-mounted overground training systems. The former one involves stepping on a motorized treadmill while a percentage of the patient's body weight is unloaded by a counterweight-harness system [3], whereas the latter one is mounted to a ceiling track so that the therapist can work hand in hand with the patient to allow personalized assistance [4]. Conventional static and passive training systems usually consist of winches, counterweights, and elastic springs [5], while recently, several robotic BWS devices have been developed to automate the assistance during gait training. For example, the Lokomat exoskeleton system uses motors to drive the patient's lower limbs based on a reference trajectory over a treadmill [6]. The LOPES [7] treadmill system provides BWS via cable-driven series elastic actuators with an impedance controller. The ceiling-mounted ZeroG system allows patients with severe gait impairment to practice gait and balance activities in a controlled manner inside a gait laboratory [4]. By unloading a certain percentage of body weight utilizing the aforementioned rehabilitation systems, patients can counteract gravity with less strength generated from their weakened muscles.

Despite the fact that robot-assisted rehabilitation systems have shown promise in improving patients' gaits, significant challenges still remain in aspects of control and mobility. The Lokomat system uses an impedance controller combined with supportive torques estimated through an adaptation algorithm, which makes the patients follow a specific joint position trajectory [6]. However, studies have shown that for subacute stroke patients, conventional labor-intensive interventions are more effective than robotic-assisted gait training using the Lokomat [8]. Although new control strategies based on potential force fields have improved the mechanical transparency of the Lokomat to encourage patient participation during training [9], these control strategies still depend on predefined reference trajectories that may not generalize well across patients. In contrast, the ceiling-mounted ZeroG system allows freedom of motion while providing constant BWS with minimum horizontal dragging force as the patient walks [4]. However, patients can only receive therapy in clinical environments with treadmill or ceiling-mounted training devices, which greatly reduces the flexibility, convenience, and frequency of the therapy. A less restrictive form of BWS might be achievable through mobile wearable control systems.

Many recent mobile powered orthoses and exoskeletons address the issue of mobility, but the vast majority of these devices compensate for chronic deficits rather than provide therapeutic assistance for gait retraining [10], [11]. Limited work has been done on mobile exoskeletons that provide weight support or gravity cancellation using active control or passive mechanical structures. Although not designed for physical rehabilitation, the BLEEX enhances the ability of an able-bodied user to carry extra heavy loads, using force control to minimize the user's interaction forces with the

Asterisk indicates corresponding author.
G. Lv* is with the Department of Electrical Engineering and R. D. Gregg is with the Departments of Bioengineering and Mechanical Engineering, University of Texas at Dallas, Richardson, TX 75080, USA. {Ge.Lv, rgregg}@utdallas.edu

This work was supported by the National Institute of Child Health & Human Development of the NIH under Award Number DP2HD080349. The content is solely the responsibility of the authors and does not necessarily represent the official views of the NIH. R. D. Gregg holds a Career Award at the Scientific Interface from the Burroughs Welcome Fund.

exoskeleton so the user does not feel the weight of the backpack [12]. However, minimizing interaction forces with the exoskeleton does not offload the body weight of the human user. The passive gravity-balancing orthosis in [13] can provide variable gravity assistance to the patient's leg in the swing period by adjusting the geometry of the links and the spring locations of the device. However, the use of physical springs makes the device too cumbersome to adjust for the progressive levels of support needed in a clinical setting. Powered orthoses/exoskeletons that provide easily adjustable BWS during both stance and swing might enable greater flexibility during gait rehabilitation, motivating the development of novel control strategies for this purpose.

Potential energy shaping control, a method that alters the dynamical characteristics of a mechanical system, could possibly be used to augment the forces from gravity perceived by the human body. Gregg et al. simulated potential energy shaping for a simple compass-gait model in [14], ignoring the underactuated degrees of freedom (DOFs) encountered during human walking. This simplification prevented translation to a real orthosis that can be used by patients. More realistic models with unactuated DOFs are needed to design orthotic control strategies that are appropriate for the behaviors of human locomotion. However, shaping the potential energy is difficult for underactuated dynamical systems since the *Matching Conditions*, whose solutions dictate the achievable forms of a system's closed-loop energy, can be quite difficult to satisfy [15]. The phases of underactuation encountered during human walking and the limited number of orthosis actuators present significant challenges to consistently matching a desired potential energy for the human in closed loop.

This paper develops a methodology for underactuated potential energy shaping that leverages the contact constraints encountered during human walking. Holonomic contact constraints will be defined for three phases of stance to reduce the number of unactuated DOFs in equivalent constrained dynamics, by which we will satisfy the matching conditions corresponding to weight-shaped potential energy. We begin in Section II by modeling the contact constraints for four phases of gait: heel contact, flat foot, toe contact, and no contact (i.e., swing). In Section III the matching condition is derived and satisfied to obtain energy shaping control laws for each contact phase. Simulations of an 8-DOF biped in Section IV demonstrate that the proposed controllers result in shorter and slower steps accompanied by higher swing foot clearance during swing period. These results suggest that the proposed orthotic control strategy could provide variable weight augmentation for mobile gait training.

II. Dynamics of the Biped

In this section, we are interested in controlling a powered knee-ankle orthosis using only feedback local to its leg. For the purpose of control derivation, we separate the dynamical models of the stance and swing legs, which are coupled through interaction forces (Fig. 1). We also assume the masses m_i, $i \in \{\mathrm{f}, \mathrm{s}, \mathrm{t}, \mathrm{h}\}$, shown in Fig. 1 are the combined masses of the human limb and its orthosis.

A. Stance Leg

The stance leg is modeled as a kinematic chain with respect to an inertial reference frame (IRF) defined at either the heel or toe, depending on the phase of the stance period (to be discussed later). The configuration of this leg is given by $q_{\mathrm{st}} = (p_{\mathrm{x}}, p_{\mathrm{y}}, \phi, \theta_{\mathrm{a}}, \theta_{\mathrm{k}})^T$, where p_{x} and p_{y} are the Cartesian coordinates of the heel, ϕ is the absolute angle of the heel defined with respect to the vertical axis, and θ_{a} and θ_{k} are the angles of the ankle and knee, respectively. The Lagrangian dynamics can be derived in the form

$$M_{\mathrm{st}}(q_{\mathrm{st}})\ddot{q}_{\mathrm{st}} + C_{\mathrm{st}}(q_{\mathrm{st}}, \dot{q}_{\mathrm{st}})\dot{q}_{\mathrm{st}} + N_{\mathrm{st}}(q_{\mathrm{st}}) + A_\ell(q_{\mathrm{st}})^T\lambda = B_{\mathrm{st}}u_{\mathrm{st}} + B_{\mathrm{st}}v_{\mathrm{st}} + J_{\mathrm{st}}(q_{\mathrm{st}})^T F, \quad (1)$$

where M_{st} is the inertia/mass matrix, C_{st} is the Coriolis/centrifugal matrix, and N_{st} is the gravitational forces vector. The constraint matrix $A_\ell \in \mathbb{R}^{c\times 5}$ is defined as the gradient of the constraint functions, where the number of contact constraints, c, depends on the contact condition indicated by $\ell \in \{\mathrm{heel}, \mathrm{flat}, \mathrm{toe}\}$. The Lagrange multiplier λ is calculated using the method in [16]. Assuming the orthosis has actuation at the ankle and knee joints, i.e., $u_{\mathrm{st}} = [u_{\mathrm{a}}, u_{\mathrm{k}}]^T \in \mathbb{R}^{2\times 1}$, where u_{a} and u_{k} are the torques at the ankle and knee joints, the matrix $B_{\mathrm{st}} = (0_{2\times 3}, I_{2\times 2})^T$ maps joint torques into the coordinate system. The interaction forces $F = (F_{\mathrm{x}}, F_{\mathrm{y}}, M_{\mathrm{z}})^T \in \mathbb{R}^{3\times 1}$ between the hip of stance model and the swing thigh are composed of 3 parts: two linear forces and a moment in the sagittal plane [16]. Force vector F is mapped into the system's dynamics by the *body Jacobian* matrix $J_{\mathrm{st}}(q_{\mathrm{st}}) \in \mathbb{R}^{3\times 5}$. The human input term $v_{\mathrm{st}} = [v_{\mathrm{ha}}, v_{\mathrm{hk}}]^T \in \mathbb{R}^{2\times 1}$ provides additional torques at the ankle and knee joints, i.e., v_{ha} and v_{hk}. While designing the energy shaping controller, we make no assumptions about the human input term or interaction forces.

During stance phase, the locomotion of the stance leg can be separated into three sub-phases: heel contact, flat foot, and toe contact, as depicted in Fig. 2, for which holonomic contact constraints can be appropriately defined.

1) Heel Contact: During heel contact, the heel is fixed to the ground as the only contact point, about which the stance leg rotates. The IRF is defined at the heel, yielding the constraint $a_{\mathrm{heel}}(q) = 0$ and the constraint matrix $A_{\mathrm{heel}} = \nabla_q a_{\mathrm{heel}}$ where

$$a_{\mathrm{heel}} := (p_{\mathrm{x}}, p_{\mathrm{y}})^T, \quad (2)$$

$$A_{\mathrm{heel}} = \left(I_{2\times 2}, 0_{2\times 3}\right).$$

2) Flat Foot: At this configuration, the foot is flat on the ground slope, where ϕ is equal to the slope angle. The IRF is still defined at the heel, which yields the constraint $a_{\mathrm{flat}}(q) = 0$ and the constraint matrix $A_{\mathrm{flat}} = \nabla_q a_{\mathrm{flat}}$ where

$$a_{\mathrm{flat}} := (p_{\mathrm{x}}, p_{\mathrm{y}}, \phi - \gamma)^T, \quad (3)$$

$$A_{\mathrm{flat}} = \left(I_{3\times 3}, 0_{3\times 2}\right).$$

3) Toe Contact: The toe contact condition begins when the Center of Pressure (COP), the point along the foot where the ground reaction force is imparted, reaches the toe. During this phase the toe is the only contact point, about which the stance leg rotates. The IRF is defined at this contact point to simplify the contact constraints. The coordinates of the heel are then defined with respect to the toe, which gives us the constraint $a_{\text{toe}}(q) = 0$ and the constraint matrix $A_{\text{toe}} = \nabla_q a_{\text{toe}}$ where

$$a_{\text{toe}} := (p_{\text{x}} - l_{\text{f}}\cos(\phi), p_{\text{y}} - l_{\text{f}}\sin(\phi))^T, \tag{4}$$
$$A_{\text{toe}} = \begin{pmatrix} 1 & 0 & l_{\text{f}}\sin(\phi) & 0 & 0 \\ 0 & 1 & -l_{\text{f}}\cos(\phi) & 0 & 0 \end{pmatrix}.$$

B. Swing Leg

We choose the hip as a floating base for the swing leg's kinematic chain in Fig. 1. The full configuration of this leg is given as $q_{sw} = (h_{\text{x}}, h_{\text{y}}, \theta_{\text{th}}, \theta_{\text{sk}}, \theta_{\text{sa}})^T$, where h_{x} and , h_{y} are the positions of the hip, θ_{th} is the absolute angle defined between the vertical axis and the swing thigh, and θ_{sk} and θ_{sa} are the angles of the swing knee and ankle, respectively. By deriving the equations of motion, we obtain

$$M_{\text{sw}}(q_{\text{sw}})\ddot{q}_{\text{sw}} + C_{\text{sw}}(q_{\text{sw}}, \dot{q}_{\text{sw}})\dot{q}_{\text{sw}} + N_{\text{sw}}(q_{\text{sw}}) = B_{\text{sw}}u_{\text{sw}} + B_{\text{sw}}v_{\text{sw}} - J_{\text{sw}}(q_{\text{sw}})^T F, \tag{5}$$

where M_{sw} is the inertia/mass matrix, C_{sw} is the Coriolis/centrifugal matrix, N_{sw} is the gravitational forces vector. The matrix $B_{\text{sw}} = (0_{2\times3}, I_{2\times2})^T$ maps the orthosis torque vector $u_{\text{sw}} = [u_{\text{sk}}, u_{\text{sa}}]^T \in \mathbb{R}^{2\times1}$ into the system, where u_{sk} and u_{sa} are the torques at the swing knee and swing ankle, respectively. The vector $F = (F_{\text{x}}, F_{\text{y}}, M_{\text{z}})^T \in \mathbb{R}^{3\times1}$ contains the interaction forces between the swing leg and hip (including human hip torques), and $J_{\text{sw}}(q_{\text{sw}}) \in \mathbb{R}^{3\times5}$ is the *body Jocabian* matrix that maps F into the dynamics. The input vector $v_{\text{sw}} = [v_{\text{hsk}}, v_{\text{hsa}}]^T \in \mathbb{R}^{2\times1}$ contains human knee and ankle torques v_{hsk} and v_{hsa}, respectively. As in the case of stance leg, we design the energy shaping controller without assumptions on the human input term or interaction forces. There are no contact constraints during swing, i.e., $A_{\text{sw}} = 0$.

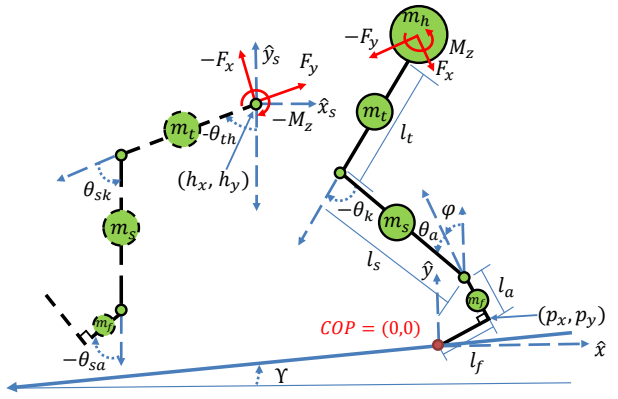

Fig. 1. Kinematic model of the biped, where the stance leg is shown in solid black and the swing leg in dashed black. For simulation study, we assume the biped is walking on a slope with angle γ.

III. Energy Shaping Control

A. Definition of Matching Condition

Consider a forced Euler-Lagrange system with configuration space $\mathbb{Q}$, taken for simplicity to be equal to $\mathbb{R}^n$, and described by a Lagrangian $L : T\mathbb{Q} \to \mathbb{R}$ [17]:

$$\frac{d}{dt}\partial_{\dot{q}}L(q,\dot{q}) - \partial_q L(q,\dot{q}) = B(q)u + F_{nc}, \tag{6}$$

where $B(q) : \mathbb{R}^m \to T_q{}^*\mathbb{Q} \simeq \mathbb{R}^n$ with rank m maps the control torque $u \in \mathbb{R}^m$ into the dynamical system. We only consider the underactuated case, i.e., $m < n$, and $F_{nc} \in \mathbb{R}^n$ contains the external (non-conservative) forces. We can express (6) in the following form for a mechanical system:

$$M(q)\ddot{q} + C(q,\dot{q})\dot{q} + N(q) = B(q)u + F_{nc}, \tag{7}$$

where terms on the left-hand side are defined similarly to (1). Consider another unforced Euler-Lagrange system defined by a Lagrangian $\tilde{L} : T\mathbb{Q} \to \mathbb{R}$:

$$\frac{d}{dt}\partial_{\dot{q}}\tilde{L}(q,\dot{q}) - \partial_q \tilde{L}(q,\dot{q}) = F_{nc}, \tag{8}$$

where the corresponding Lagrangian dynamics are given as

$$M(q)\ddot{q} + C(q,\dot{q})\dot{q} + \tilde{N}(q) = F_{nc}. \tag{9}$$

The system (7) and system (9) *match* if there exists a full-rank left annihilator $B(q)^\perp \in \mathbb{R}^{(n-m)\times n}$ of $B(q)$, i.e., $B(q)^\perp B(q) = 0$ and $\text{rank}(B(q)^\perp) = (n-m)$, $\forall q \in \mathbb{Q}$, such that [17]

$$B(q)^\perp(N - \tilde{N}) = 0. \tag{10}$$

Assuming (10) is satisfied, the control law that achieves the closed-loop dynamics (9) is given as

$$u = (B^T B)^{-1}B^T(N - \tilde{N}), \tag{11}$$

where $\tilde{N}$ is the desired gravitational forces vector. We will choose $\tilde{N}$ with beneficial properties such as weight reduction.

B. Equivalent Constrained Dynamics

The DOFs of a dynamical system can be reduced with holonomic constraints, such as contact constraints. We will define the matching condition for the equivalent constrained dynamics, which are (1) with A and λ embedded to obtain the form of (7). Constraint matrices are defined for each configuration in Section II-A, and we calculate λ based on the results in [16] and [18] as

$$\begin{aligned} \lambda &= \hat{\lambda} + \tilde{\lambda}u_{\text{st}} + \bar{\lambda}F, \\ \hat{\lambda} &= W(\dot{A}_\ell \dot{q}_{\text{st}} - A_\ell M_{\text{st}}^{-1}(C_{\text{st}}\dot{q}_{\text{st}} + N_{\text{st}} - B_{\text{st}}v_{\text{st}})), \\ \tilde{\lambda} &= W A_\ell M_{\text{st}}^{-1} B_{\text{st}}, \\ \bar{\lambda} &= W A_\ell M_{\text{st}}^{-1} J_{\text{st}}^T, \\ W &= (A_\ell M_{\text{st}}^{-1} A_\ell^T)^{-1}. \end{aligned} \tag{12}$$

Plugging in λ, dynamics (1) become:

$$M_\lambda \ddot{q}_{\text{st}} + C_\lambda \dot{q}_{\text{st}} + N_\lambda = B_\lambda u_{\text{st}} + B_\lambda v_{\text{st}} + J_\lambda^T F, \tag{13}$$

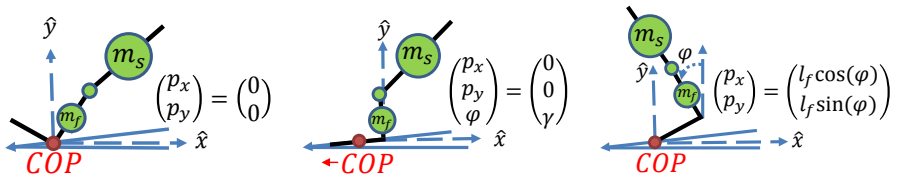

Fig. 2. Heel contact configuration (left), flat foot configuration (center), and toe contact configuration (right) during stance phase on a slope with angle γ.

where

$$\begin{aligned} M_\lambda &= M_{\text{st}}, \\ C_\lambda &= [I - A_\ell^T W A_\ell M_{\text{st}}^{-1}] C_{\text{st}} + A_\ell^T W \dot{A}_\ell, \\ B_\lambda &= [I - A_\ell^T W A_\ell M_{\text{st}}^{-1}] B_{\text{st}}, \\ N_\lambda &= [I - A_\ell^T W A_\ell M_{\text{st}}^{-1}] N_{\text{st}}, \\ J_\lambda &= J_{\text{st}} [I - A_\ell^T W A_\ell M_{\text{st}}^{-1}]^T. \end{aligned} \tag{14}$$

We wish to achieve in closed-loop the equivalent constrained dynamics

$$M_\lambda \ddot{q}_{\text{st}} + C_\lambda \dot{q}_{\text{st}} + \tilde{N}_\lambda = B_\lambda v_{\text{st}} + J_\lambda^T F, \tag{15}$$

where we choose

$$\tilde{N}_\lambda = [I - A_\ell^T W A_\ell M_{\text{st}}^{-1}] \tilde{N}_{\text{st}} \tag{16}$$

given the desired gravitational forces vector $\tilde{N}_{\text{st}}$, which will be introduced in Section III-C for each configuration. Given that (13) and (15) have the form of (7) and (9), respectively, the equivalent constrained matching condition has the same form as (10):

$$B_\lambda^\perp (N_\lambda - \tilde{N}_\lambda) = 0, \tag{17}$$

and the control law that achieves (15) is similarly given as

$$u_{\text{st}} = (B_\lambda^T B_\lambda)^{-1} B_\lambda^T (N_\lambda - \tilde{N}_\lambda). \tag{18}$$

In the next section, we will plug A_ℓ into (14) to obtain B_λ for each contact condition. Then, choosing the annihilators for each B_λ, we will satisfy the matching condition and derive the corresponding control law with desired $\tilde{N}_\lambda$ based on (17) and (18).

C. Matching Conditions for Stance

1) Blockwise Inversion for M_{st}: In order to derive the equivalent constrained dynamics, we need to decompose M_{st}^{-1}, which can be easily done using the blockwise inversion method introduced in [19]. To begin we decompose M_{st} into four submatrices:

$$M_{\text{st}} = \begin{pmatrix} M_1 & M_2 \\ M_3 & M_4 \end{pmatrix}, \tag{19}$$

where M_1 and M_4 are square and $M_3 = M_2^T$. Given that inertia matrices are non-singular [18], the inverse of M_{st} can be obtained as

$$\begin{pmatrix} \Delta^{-1} & -\Delta^{-1} M_2 M_4^{-1} \\ -M_4^{-1} M_3 \Delta^{-1} & M_4^{-1} + M_4^{-1} M_3 \Delta^{-1} M_2 M_4^{-1} \end{pmatrix}, \tag{20}$$

where $\Delta = (M_1 - M_2 M_4^{-1} M_3)$.

We can use this inversion method if and only if M_4 and Δ are nonsingular. We can treat M_4 as an inertia matrix for a subsystem with lower DOFs based on the results in [20], which proves that M_4 is nonsingular since an inertia matrix is symmetric and positive-definite [18]. Using the formulas of Schur in [21] to calculate the determinant of M_{st}, we have

$$\det(M_{\text{st}}) = \det(M_4) \det(\Delta).$$

Since $\det(M_{\text{st}}) \neq 0$ and $\det(M_4) \neq 0$, we have $\det(\Delta) \neq 0$ by [21], which proves that Δ is nonsingular.

2) Heel Contact: At this configuration, let $M_1 \in \mathbb{R}^{2\times 2}$, $M_2 \in \mathbb{R}^{2\times 3}$, $M_3 \in \mathbb{R}^{3\times 2}$, $M_4 \in \mathbb{R}^{3\times 3}$ so that the multiplication of A_{heel} and M_{st}^{-1} can be greatly simplified. We plug A_{heel} into (14) using the decomposition of M_{st}^{-1} from (20) to obtain

$$[I - A_{\text{heel}}^T W A_{\text{heel}} M_{\text{st}}^{-1}] = \begin{pmatrix} 0_{2\times 2} & M_2 M_4^{-1} \\ 0_{3\times 2} & I_{3\times 3} \end{pmatrix}. \tag{21}$$

Let $V_1 = [V_{11},\ V_{12}] = M_2 M_4^{-1}$, where $V_{11} \in \mathbb{R}^{2\times 1}$ and $V_{12} \in \mathbb{R}^{2\times 2}$. Plugging B_{st} and (21) into (14), we have

$$B_{\lambda 1} = \begin{bmatrix} V_1 B_{\text{st}(3,5)} \\ B_{\text{st}(3,5)} \end{bmatrix} = \begin{bmatrix} V_{12} \\ 0_{1\times 2} \\ I_{2\times 2} \end{bmatrix}, \tag{22}$$

$$N_{\lambda 1} = \begin{bmatrix} V_1 N_{\text{st}(3,5)} \\ N_{\text{st}(3,5)} \end{bmatrix} = \begin{bmatrix} V_{11} N_{\text{st}(3,3)} + V_{12} N_{\text{st}(4,5)} \\ N_{\text{st}(3,3)} \\ N_{\text{st}(4,5)} \end{bmatrix},$$

where subscript (i, j) indicates rows i through j of a matrix. Because we constrained the first two DOFs to zero in (2), the first two rows of B_{st} disappear in $B_{\lambda 1}$ and $N_{\lambda 1}$.

Let $\tilde{N}_{\lambda 1}$ be the desired (constrained) gravitational forces vector defined by (16). We will choose $\tilde{N}_{\text{st}}$ in (16) by replacing the shank, thigh, and hip masses[1] in N_{st} with $\tilde{m}_i < m_i$, $i \in \{\text{s}, \text{t}, \text{h}\}$. Then, we wish to satisfy the matching condition

$$B_{\lambda 1}^\perp (N_{\lambda 1} - \tilde{N}_{\lambda 1}) = 0_{3\times 1}. \tag{23}$$

We choose the annihilator of $B_{\lambda 1}$ as

$$B_{\lambda 1}^\perp = \begin{bmatrix} I_{2\times 2} & 0_{2\times 1} & -V_{12} \\ 0_{1\times 2} & 1 & 0_{1\times 2} \end{bmatrix}. \tag{24}$$

It is obvious that $B_{\lambda 1}^\perp B_{\lambda 1} = 0$ and $\text{rank}(B_{\lambda 1}^\perp) = 3$. Plugging terms into (23), the matching condition holds if $\tilde{N}_{\text{st}(3,3)} = N_{\text{st}(3,3)}$, i.e., not shaping the heel orientation DOF. Assuming this case in (16), we can achieve $\tilde{N}_{\lambda 1}$ in the closed-loop dynamics with the control law

$$u_{\text{heel}} = (B_{\lambda 1}^T B_{\lambda 1})^{-1} B_{\lambda 1}^T (N_{\lambda 1} - \tilde{N}_{\lambda 1}). \tag{25}$$

[1]The upper body segments are lumped into a single point mass at the hip in the stance dynamics. We can only shape the masses of the stance shank, thigh, and hip in the gravitational forces vector with orthosis actuators located at the ankle and knee.

The fact that $B_{\lambda 1}$ and $N_{\lambda 1}$ are functions of q implies that u_{heel} only requires position feedback, which will be beneficial for experimental implementation. We will see that this is also true for the other two configurations of stance and the swing configuration.

3) Flat Foot: At this configuration, let $M_1 \in \mathbb{R}^{3\times 3}, M_2 \in \mathbb{R}^{3\times 2}, M_3 \in \mathbb{R}^{2\times 3}, M_4 \in \mathbb{R}^{2\times 2}$, which have different dimensions than the previous case in order to handle three contact constraints instead of two. Plugging A_{flat} into (14) using the decomposition of M_{st}^{-1} from (20), we obtain

$$B_{\lambda 2} = \begin{bmatrix} V_2 \\ I_{2\times 2} \end{bmatrix}, \; N_{\lambda 2} = \begin{bmatrix} V_2 N_{\text{st}(4,5)} \\ N_{\text{st}(4,5)} \end{bmatrix}, \tag{26}$$

where $V_2 = M_2 M_4^{-1} \in \mathbb{R}^{3\times 2}$, and $N_{\text{st}(4,5)}$ contains the last two rows of N_{st}.

We replace masses in $N_{\text{st}(4,5)}$ to define $\tilde{N}_{\lambda 2}$ based on (16) and the corresponding matching condition is

$$B_{\lambda 2}^{\perp}(N_{\lambda 2} - \tilde{N}_{\lambda 2}) = 0_{3\times 1}. \tag{27}$$

Choosing the annihilator of $B_{\lambda 2}$ as

$$B_{\lambda 2}^{\perp} = \begin{bmatrix} I_{3\times 3}, & -V_2 \end{bmatrix}, \tag{28}$$

where $B_{\lambda 2}^{\perp} B_{\lambda 2} = 0$ and $\text{rank}(B_{\lambda 2}^{\perp}) = 3$, we immediately see that the matching condition holds. The corresponding energy shaping control law is given as

$$u_{\text{flat}} = (B_{\lambda 2}^T B_{\lambda 2})^{-1} B_{\lambda 2}^T (N_{\lambda 2} - \tilde{N}_{\lambda 2}). \tag{29}$$

4) Toe Contact: At the toe contact configuration, even though this configuration has the same number of constraints as defined in the *Heel Contact* case, we decompose M_{st} as in the *Flat Foot* case to simplify the derivation. Plugging A_{toe} into (14) using the decomposition of M_{st}^{-1} from (20), we obtain

$$B_{\lambda 3} = \begin{bmatrix} V_4 \\ I_{2\times 2} \end{bmatrix}, \; N_{\lambda 3} = \begin{bmatrix} V_3 N_{\text{st}(1,3)} + V_4 N_{\text{st}(4,5)} \\ N_{\text{st}(4,5)} \end{bmatrix}, \tag{30}$$

where $N_{\text{st}(1,3)}$ and $N_{\text{st}(4,5)}$ are the first three and last two rows of N_{st}, respectively. We split up N_{st} in this way because the upper-left part of (20) is no longer zero, and V_3 and V_4 are defined as

$$V_3 = I_{3\times 3} - U, \quad V_4 = U M_2 M_4^{-1}, \tag{31}$$

where U is given as

$$U = r^T (r\Delta^{-1} r^T)^{-1} r\Delta^{-1},$$
$$r = \begin{pmatrix} 1 & 0 & l_f \sin(\phi) \\ 0 & 1 & -l_f \cos(\phi) \end{pmatrix}.$$

We replace the mass terms in N_{st} to define $\tilde{N}_{\lambda 3}$ from (16), and we choose the annihilator of $B_{\lambda 3}$ as

$$B_{\lambda 3}^{\perp} = \begin{bmatrix} I_{3\times 3}, & -V_4 \end{bmatrix}, \tag{32}$$

where $B_{\lambda 3}^{\perp} B_{\lambda 3} = 0$ and $\text{rank}(B_{\lambda 3}^{\perp}) = 3$.

Plugging in (30) and (32), the left-hand side of the matching condition is

$$B_{\lambda 3}^{\perp}(N_{\lambda 3} - \tilde{N}_{\lambda 3}) = V_3(N_{\text{st}(1,3)} - \tilde{N}_{\text{st}(1,3)}). \tag{33}$$

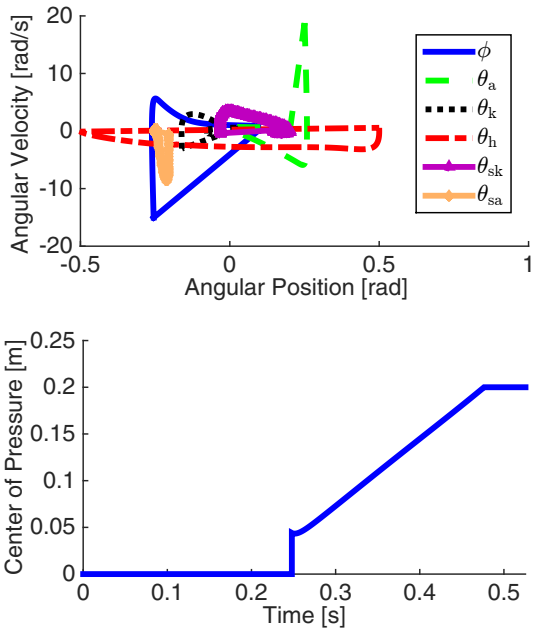

Fig. 3. Phase portrait (top) and Center of Pressure (bottom) of the stable gait with impedance control during one step period.

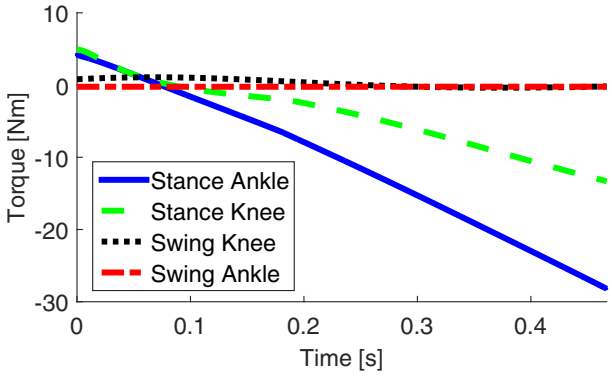

Fig. 4. Energy shaping control torques with 24.5% BWS during one step.

Therefore, the matching condition is not immediately satisfied. If we assume $N_{\text{st}(1,3)} = \tilde{N}_{\text{st}(1,3)}$, which means we are not shaping the unactuated DOFs (two of which are already constrained) in this configuration, the matching condition will hold. The corresponding energy shaping control law is

$$u_{\text{toe}} = (B_{\lambda 3}^T B_{\lambda 3})^{-1} B_{\lambda 3}^T (N_{\lambda 3} - \tilde{N}_{\lambda 3}), \tag{34}$$

where $\tilde{N}_{\lambda 3} = \begin{bmatrix} V_3 N_{\text{st}(1,3)} + V_4 \tilde{N}_{\text{st}(4,5)} \\ \tilde{N}_{\text{st}(4,5)} \end{bmatrix}$.

D. Matching Condition for Swing

For the swing leg, there are no contact constraints defined in the dynamics. Hence, we can directly derive the matching condition from (5). The swing shank mass m_{s} and swing foot mass m_{f} will be shaped by the swing controller, i.e., choosing $\tilde{m}_i < m_i$, $i \in \{\text{f}, \text{s}\}$ in $\tilde{N}_{\text{sw}}$.

Letting $B_{\text{sw}}^{\perp} = [I_{3\times 3}, 0_{3\times 2}]$, we know $B_{\text{sw}}^{\perp} B_{\text{sw}} = 0$ and $\text{rank}(B_{\text{sw}}^{\perp}) = 3$. The left-hand side of the matching condition in (10) is

$$B_{\text{sw}}^{\perp}(N_{\text{sw}} - \tilde{N}_{\text{sw}}) = (N_{\text{sw}(1,3)} - \tilde{N}_{\text{sw}(1,3)}),$$

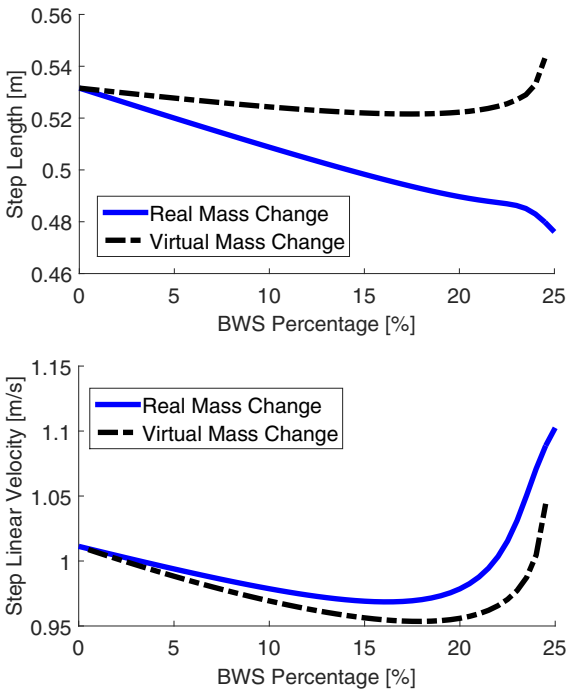

Fig. 5. Step length (top) and step linear velocity (bottom) with 0% to 25% BWS and real mass change.

TABLE I
MODEL AND SIMULATION PARAMETERS

Parameter	Variable	Value
Hip mass	m_{h}	31.73 [kg]
Thigh mass	m_{t}	9.457 [kg]
Shank mass	m_{s}	4.053 [kg]
Foot mass	m_{f}	1 [kg]
Thigh moment of inertia	I_{t}	0.1995 [kg·m^2]
Shank moment of inertia	I_{s}	0.0369 [kg·m^2]
Full biped shank length	l_{s}	0.428 [m]
Full biped thigh length	l_{t}	0.428 [m]
Full biped heel length	l_{a}	0.07 [m]
Full biped foot length	l_{f}	0.2 [m]
Slope angle	γ	0.095 [rad]
Hip equilibrium angle	$\theta_{\mathrm{h}}^{\mathrm{eq}}$	0.2 [rad]
Hip proportional gain	K_{ph}	182.258 [N·m/rad]
Hip derivative gain	K_{dh}	18.908 [N·m·s/rad]
Swing knee equilibrium angle	$\theta_{\mathrm{sk}}^{\mathrm{eq}}$	0.2 [rad]
Swing knee proportional gain	K_{psk}	182.258 [N·m/rad]
Swing knee derivative gain	K_{dsk}	18.908 [N·m·s/rad]
Swing ankle equilibrium angle	$\theta_{\mathrm{sa}}^{\mathrm{eq}}$	-0.25 [rad]
Swing ankle proportional gain	K_{psa}	182.258 [N·m/rad]
Swing ankle derivative gain	K_{dsa}	0.802 [N·m·s/rad]
Stance ankle equilibrium angle	$\theta_{\mathrm{a}}^{\mathrm{eq}}$	0.01 /rad]
Stance ankle proportional gain	K_{pa}	546.774 [N·m/rad]
Stance ankle derivative gain	K_{da}	21.257 [N·m·s/rad]
Stance knee equilibrium angle	$\theta_{\mathrm{k}}^{\mathrm{eq}}$	-0.05 [rad]
Stance knee proportional gain	K_{pk}	546.774 [N·m/rad]
Stance knee derivative gain	K_{dk}	21.257 [N·m·s/rad]

where $\tilde{N}_{\mathrm{sw}}$ is the desired gravitational forces vector, and $N_{\mathrm{sw}(1,3)}$ and $\tilde{N}_{\mathrm{sw}(1,3)}$ are the first three rows of N_{sw} and $\tilde{N}_{\mathrm{sw}}$, respectively. Therefore, the matching condition can only be satisfied if the first three rows[2] of N_{sw} (corresponding to unactuated inertial DOFs) are unshaped, i.e., $N_{\mathrm{sw}(1,3)} = \tilde{N}_{\mathrm{sw}(1,3)}$. This is reasonable because swing leg masses can only be shaped by actuators that react against proximal links (the thigh). The swing controller for the orthosis is then

$$u_{\mathrm{sw}} = (B_{\mathrm{sw}}^T B_{\mathrm{sw}})^{-1} B_{\mathrm{sw}}^T (N_{\mathrm{sw}} - \tilde{N}_{\mathrm{sw}}), \tag{35}$$

where $\tilde{N}_{\mathrm{sw}} = [N_{\mathrm{sw}(1,3)}^T, \tilde{N}_{\mathrm{sw}(4,5)}^T]^T$.

IV. SIMULATIONS AND RESULTS

Now that we have designed controllers for the orthosis, we wish to study it during simulated walking with the full biped model, i.e, combing the stance and swing leg together in Fig. 1. This requires us to consider the coupled dynamics of the two legs [22]. The full biped model's configuration space is given as $q_{\mathrm{e}} = (q_{\mathrm{st}}^T, \theta_{\mathrm{h}}, \theta_{\mathrm{sk}}, \theta_{\mathrm{sa}})^T$, where θ_{h} is defined as the hip angle between the stance and swing thigh. For simplicity we assume symmetry in the full biped, i.e., two identical orthoses on both human legs [16].

A. Human Inputs

In order to predict the effects of the energy shaping controller on human locomotion, we must first construct a human-like, stable walking gait in simulation. According to the results shown in [23], a simulated 7-link biped can converge to a stable, natural-looking gait using joint impedance control. The control torque of each joint can be constructed from an energetically passive spring-damper coupled with phase-dependent equilibrium points [24]. We adopt this control paradigm to generate dynamic walking gaits that preserve the ballistic swing motion [25] and the energetic efficiency down slopes [26] that are characteristic of human locomotion. We assume that the human has input torques at the ankle, knee and hip joints of both legs. The total input torque vector, i.e., orthotic inputs + human inputs, for the full biped model is given as

$$\begin{aligned} \tau &= (B_{\mathrm{st}}^T, 0_{2\times 3})^T u_\ell + (0_{2\times 3}, B_{\mathrm{sw}}^T)^T u_{\mathrm{sw}} + v_{\mathrm{h}}, \\ v_{\mathrm{h}} &= [0_{1\times 3}, v_{\mathrm{ha}}, v_{\mathrm{hk}}, v_{\mathrm{hh}}, v_{\mathrm{hsk}}, v_{\mathrm{hsa}}]^T \in \mathbb{R}^{8\times 1}, \end{aligned} \tag{36}$$

where $\ell \in \{\mathrm{heel}, \mathrm{flat}, \mathrm{toe}\}$ indicates the stance controller based on the contact condition, and v_{h} is the vector of human inputs. The human torque for a single joint in v_{h} is given by

$$v_{\mathrm{h}j} = -K_{pj}(\theta_j - \theta_j^{\mathrm{eq}}) - K_{dj}\dot{\theta}_j, \tag{37}$$

where $K_{\mathrm{p}j}$, $K_{\mathrm{d}j}$, θ_j^{eq} respectively correspond to the stiffness, viscosity, and equilibrium angle of joint $j \in \{\mathrm{a}, \mathrm{k}, \mathrm{h}, \mathrm{sk}, \mathrm{sa}\}$.

B. Hybrid Dynamics

Biped locomotion is a hybrid dynamical system which includes continuous and discrete dynamics. Impacts happen when the swing heel contacts the ground, and when contact constraints change between the heel contact and flat foot configurations defined in Section II-A. The corresponding impact equations map the state of the biped at the instant before impact to the state at the instant after impact. Note that no impact occurs when switching between the flat foot and toe contact configurations, but the location of the IRF

[2]With orthosis actuators at the swing ankle and swing knee, we can only shape the swing shank and swing foot masses in N_{sw}.

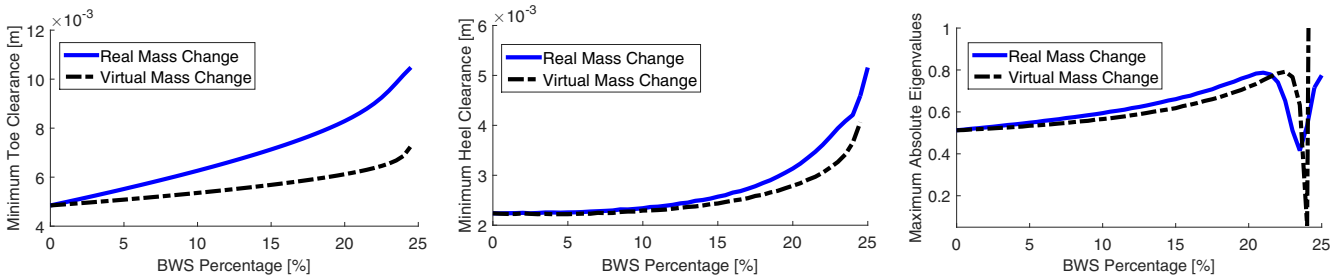

Fig. 6. Minimum toe and heel clearances during swing (left, center), maximum absolute eigenvalues (right) from 0% to 25% BWS and real mass change.

does change from heel to toe. Based on the results in [16], the hybrid dynamics and impact maps during one step are computed in the following sequence:

$$
\begin{aligned}
&1. \quad M_{\mathrm{e}}\ddot{q}_{\mathrm{e}} + T_{\mathrm{e}} + A_{\mathrm{e_{heel}}}^{T}\lambda_{\mathrm{e}} = \tau && \text{if} \quad a_{\mathrm{e_{flat}}} \neq 0,\\
&2. \quad \dot{q}_{\mathrm{e}}^{+} = (I - X(A_{\mathrm{e_{flat}}}X)^{-1}A_{\mathrm{e_{flat}}})\dot{q}_{\mathrm{e}}^{-} && \text{if} \quad a_{\mathrm{e_{flat}}} = 0,\\
&3. \quad M_{\mathrm{e}}\ddot{q}_{\mathrm{e}} + T_{\mathrm{e}} + A_{\mathrm{e_{flat}}}^{T}\lambda_{\mathrm{e}} = \tau && \text{if} \quad |c_p(q,\dot{q})| < l_{\mathrm{f}},\\
&4. \quad \dot{q}_{\mathrm{e}}^{+} = \dot{q}_{\mathrm{e}}^{-}, (q_{\mathrm{e}}(1)^{+}, q_{\mathrm{e}}(2)^{+})^{T} = \mathcal{G} && \text{if} \quad |c_p(q,\dot{q})| = l_{\mathrm{f}},\\
&5. \quad M_{\mathrm{e}}\ddot{q}_{\mathrm{e}} + T_{\mathrm{e}} + A_{\mathrm{e_{toe}}}^{T}\lambda_{\mathrm{e}} = \tau && \text{if} \quad h(q_{\mathrm{e}}) \neq 0,\\
&6. \quad (q_{\mathrm{e}}^{+}, \dot{q}_{\mathrm{e}}^{+}) = \Theta(q_{\mathrm{e}}^{-}, \dot{q}_{\mathrm{e}}^{-}) && \text{if} \quad h(q_{\mathrm{e}}) = 0,
\end{aligned}
$$

where the subscript e indicates the dynamics of the full biped model, $X = M_{\mathrm{e}}^{-1}A_{\mathrm{e_{flat}}}^{T}$, and $\mathcal{G} = (l_f\cos(\gamma), l_f\sin(\gamma))^{T}$ models the change in IRF. The vector $c_p(q,\dot{q})$ is the COP defined with respect to the heel IRF calculated using the conservation law of momentum. The vector T_{e} groups the Coriolis/centrifugal terms and gravitational forces for brevity. The ground clearance of the swing heel is denoted as $h(q_{\mathrm{e}})$ and Θ denotes the swing heel ground-strike impact map. The aforementioned sequence of continuous and discrete dynamics repeats after a complete step, i.e., phase 6 switches back to phase 1 for the next step.

The stability of a hybrid dynamical system can be analyzed following the method in [27]. Letting $x_{\mathrm{e}} = (q_{\mathrm{e}}^{T}, \dot{q}_{\mathrm{e}}^{T})^{T}$ be the state vector of the full biped, walking gaits are cyclic and correspond to solution curves $x_{\mathrm{e}}(t)$ of the hybrid system such that $x_{\mathrm{e}}(t) = x_{\mathrm{e}}(t+T)$, for all $t \geq 0$ and some minimal $T > 0$. These solutions, known as *hybrid periodic orbits*, correspond to equilibria of the *Poincaré* map $P : G \to G$, where $G = \{x_{\mathrm{e}} | h(q_{\mathrm{e}}) = 0\}$ is the switching surface indicating initial heel contact [16]. A periodic solution $x_{\mathrm{e}}(t)$ has a fixed point $x_{\mathrm{e}}^{*} = P(x_{\mathrm{e}}^{*})$, and we can linearize the Poincaré map about this point to analyze the local stability of the hybrid dynamical system. If the eigenvalues are within the unit circle, then the discrete system is *locally exponentially stable* (LES), and we conclude that the hybrid periodic orbit is also LES. We can numerically calculate these eigenvalues through a perturbation analysis as described in [27] after walking several steps (e.g., 24) to ensure convergence to a fixed point with any given controller.

C. Results and Discussion

We chose the model parameters of Table I to consist of average values from adult males reported in [28], with the trunk masses grouped at the hip as in [22]. Because the BWS controllers can directly compensate for the masses of the orthoses, we neglected these masses in the parameters of Table I for simplicity. The foot length was set to 0.2 m to provide reasonable amounts of time in both the flat foot and toe contact conditions. We first tuned the human impedance controller's gains to find a stable gait, where the gains are shown in Table I. The stable hybrid limit cycle is shown in the phase portrait in Fig. 3 (top), and Fig. 3 (bottom) demonstrates that the COP moves monotonically from the heel to the toe, providing a flag to detect the transition between flat foot and toe contact. After we found the nominal stable gait via impedance control, we implemented the energy shaping controller and progressively increased the BWS percentage. For notational purposes, 25% BWS corresponds to virtual masses of $\tilde{m}_i = 0.75m_i$, where $i \in \{\mathrm{s}, \mathrm{t}, \mathrm{h}\}$ for the stance leg and $i \in \{\mathrm{s}, \mathrm{f}\}$ for the swing leg. The controller's torque profile for 24.5% BWS is shown in Fig. 4.

Having achieved stable walking with a certain amount of BWS, we next demonstrated the effects of the controller for varying BWS percentages in Fig. 5 and Fig. 6. The "Real Mass Change" in these figures correspond to the true masses being changed in the physical model, whereas "Virtual Mass Change" indicates that only mass terms in the gravitational forces vector are shaped by control. We performed the aforementioned perturbations analysis when stable gaits were achieved and recorded the maximum eigenvalues of the linearized map $\nabla_{x_{\mathrm{e}}}P(x_{\mathrm{e}}^{*})$ to analyze stability. Each data point in Fig. 5 and Fig. 6 was recorded for a specific percentage of BWS after steady-state walking was achieved. This process of sequentially composing controllers to stably achieve intermediate gaits is known as *Lyapunov funneling* [14]. When changing the masses of the biped, the human impedance controller's gains were kept constant so that the effects of energy shaping could be analyzed separately. Since we are not altering the kinetic energy of the system, the simulation results of real and virtual mass shaping are not perfectly aligned, but they are close enough to reveal the effectiveness of the potential shaping approach.

From Fig. 5 we can see that from 0% to 20% BWS, the biped has smaller step lengths and velocities due to the decreasing potential energy. Patients may benefit from starting with slower and shorter steps at the beginning of therapy, and once they have gained more confidence in walking, the percentage of BWS could easily be lowered to encourage faster and longer steps. From Fig. 6 (left, middle) we can see that the swing clearances of both toe and heel

are in direct proportion to the BWS percentage. This implies that trips commonly associated with stroke gait [29] could potentially be avoided with the BWS controller.

Fig. 6 (right) shows the maximum absolute eigenvalues of $\nabla_{x_e} P(x_e^*)$. The eigenvalues tend to increase with the BWS percentage, suggesting slower local convergence rates to the associated hybrid periodic orbit. Given that gait stability is sensitive to model parameters, we can only reduce the real masses up to 25% (and the virtual masses up to 24.5%) in our passive biped model, after which there is insufficient potential energy to maintain a stable gait. However, we can make a safe assumption that patients can compensate in actual therapy as opposed to the passive simulated biped, which could possibly expand the BWS percentage applied for more substantial gait augmentation.

V. Conclusion and Future Work

We demonstrated that with the proposed methodology, potential energy shaping was achieved for underactuated biped locomotion. The closed-loop energy that can be altered via control was determined by matching conditions defined by Lagrangian dynamics that have been constrained by contact conditions. This proposed method can be used as a general framework for deriving matching conditions and subsequent control laws for any contact conditions encountered during biped locomotion. Simulation results showed that gaits can be augmented in a beneficial way for gait rehabilitation, where patients can start training with easier gaits having higher swing foot clearances to avoid tripping. Created as a rehabilitation tool, this position feedback-based controller could potentially reduce clinicians' workload and lead to a more efficient gait training process. Future work will include shaping the gravitational constant, which does not appear in the inertia matrix, and experimental implementations.

Acknowledgments

The authors thank Dr. Anne Martin for help with the COP calculations and simulation study as well as Dr. Akshay Nanjangud for editorial assistance.

References

[1] B. H. Dobkin, D. Apple, H. Barbeau, M. Basso, A. Behrman, D. Deforge, J. Ditunno, G. Dudley, R. Elashoff, L. Fugate, *et al.*, "Methods for a randomized trial of weight-supported treadmill training versus conventional training for walking during inpatient rehabilitation after incomplete traumatic spinal cord injury," *Neurorehabilitation and Neural Repair*, vol. 17, no. 3, pp. 153–167, 2003.

[2] H. Barbeau, K. Norman, J. Fung, M. Visintin, and M. Ladouceur, "Does neurorehabilitation play a role in the recovery of walking in neurological populations?" *Annals of the New York Academy of Sciences*, vol. 860, no. 1, pp. 377–392, 1998.

[3] T. G. Hornby, D. H. Zemon, and D. Campbell, "Robotic-assisted, body-weight–supported treadmill training in individuals following motor incomplete spinal cord injury," *Physical therapy*, vol. 85, no. 1, pp. 52–66, 2005.

[4] J. Hidler, D. Brennan, I. Black, D. Nichols, K. Brady, and T. Nef, "ZeroG: Overground gait and balance training system," *J. Rehabilitation Research and Development*, vol. 48, no. 4, p. 287, 2011.

[5] M. Frey, G. Colombo, M. Vaglio, R. Bucher, M. Jorg, and R. Riener, "A novel mechatronic body weight support system," *Neural Systems and Rehabilitation Engineering, IEEE Transactions on*, vol. 14, no. 3, pp. 311–321, 2006.

[6] A. Duschau-Wicke, T. Brunsch, L. Lunenburger, and R. Riener, "Adaptive support for patient-cooperative gait rehabilitation with the lokomat," in *Intelligent Robots and Systems, 2008. IROS 2008. IEEE/RSJ International Conference on*. IEEE, 2008, pp. 2357–2361.

[7] J. F. Veneman, R. Kruidhof, E. E. Hekman, R. Ekkelenkamp, E. H. Van Asseldonk, and H. Van Der Kooij, "Design and evaluation of the lopes exoskeleton robot for interactive gait rehabilitation," *Neural Systems and Rehabilitation Engineering, IEEE Transactions on*, vol. 15, no. 3, pp. 379–386, 2007.

[8] J. Hidler, D. Nichols, M. Pelliccio, K. Brady, D. D. Campbell, J. H. Kahn, and T. G. Hornby, "Multicenter randomized clinical trial evaluating the effectiveness of the lokomat in subacute stroke," *Neurorehabilitation and Neural Repair*, vol. 23, no. 1, pp. 5–13, 2009.

[9] H. Vallery, A. Duschau-Wicke, and R. Riener, "Generalized elasticities improve patient-cooperative control of rehabilitation robots," in *Rehabilitation Robotics, IEEE International Conference on*. IEEE, 2009, pp. 535–541.

[10] M. R. Tucker, J. Olivier, A. Pagel, H. Bleuler, M. Bouri, O. Lambercy, J. d. R. Millan, R. Riener, H. Vallery, and R. Gassert, "Control strategies for active lower extremity prosthetics and orthotics: a review," *J. Neuroengineering and Rehabilitation*, vol. 12, no. 1, p. 1, 2015.

[11] T. Yan, M. Cempini, C. M. Oddo, and N. Vitiello, "Review of assistive strategies in powered lower-limb orthoses and exoskeletons," *Robotics and Autonomous Systems*, vol. 64, pp. 120–136, 2015.

[12] J. Ghan, R. Steger, and H. Kazerooni, "Control and system identification for the berkeley lower extremity exoskeleton (bleex)," *Advanced Robotics*, vol. 20, no. 9, pp. 989–1014, 2006.

[13] S. K. Agrawal, S. K. Banala, A. Fattah, V. Sangwan, V. Krishnamoorthy, J. P. Scholz, and H. Wei-Li, "Assessment of motion of a swing leg and gait rehabilitation with a gravity balancing exoskeleton," *Neural Systems and Rehabilitation Engineering, IEEE Transactions on*, vol. 15, no. 3, pp. 410–420, 2007.

[14] R. D. Gregg, T. W. Bretl, and M. W. Spong, "A control theoretic approach to robot-assisted locomotor therapy," in *Decision and Control (CDC), 2010 49th IEEE Conference on*. IEEE, 2010, pp. 1679–1686.

[15] J. K. Holm and M. W. Spong, "Kinetic energy shaping for gait regulation of underactuated bipeds," in *Control Applications, 2008. IEEE International Conference on*. IEEE, 2008, pp. 1232–1238.

[16] R. D. Gregg, T. Lenzi, L. J. Hargrove, and J. W. Sensinger, "Virtual Constraint Control of a Powered Prosthetic Leg: From Simulation to Experiments with Transfemoral Amputees." *Robotics, IEEE transactions on*, vol. 30, no. 6, pp. 1455–1471, Dec. 2014.

[17] G. Blankenstein, R. Ortega, and A. J. Van Der Schaft, "The matching conditions of controlled lagrangians and ida-passivity based control," *International Journal of Control*, vol. 75, no. 9, pp. 645–665, 2002.

[18] R. M. Murray, Z. Li, S. S. Sastry, and S. S. Sastry, *A mathematical introduction to robotic manipulation*. CRC press, 1994.

[19] D. S. Bernstein, *Matrix mathematics: theory, facts, and formulas*. Princeton University Press, 2009.

[20] R. D. Gregg and M. W. Spong, "Reduction-based control of three-dimensional bipedal walking robots," *The International Journal of Robotics Research*, vol. 29, no. 6, pp. 680–702, 2010.

[21] D. V. Ouellette, "Schur complements and statistics," *Linear Algebra and its Applications*, vol. 36, pp. 187–295, 1981.

[22] R. D. Gregg and J. W. Sensinger, "Biomimetic virtual constraint control of a transfemoral powered prosthetic leg," in *American Control Conference (ACC), 2013*. IEEE, 2013, pp. 5702–5708.

[23] D. J. Braun, J. E. Mitchell, and M. Goldfarb, "Actuated dynamic walking in a seven-link biped robot," *Mechatronics, IEEE/ASME Transactions on*, vol. 17, no. 1, pp. 147–156, 2012.

[24] D. J. Braun and M. Goldfarb, "A control approach for actuated dynamic walking in biped robots," *Robotics, IEEE Transactions on*, vol. 25, no. 6, pp. 1292–1303, 2009.

[25] S. Mochon and T. A. McMahon, "Ballistic walking," *J. biomechanics*, vol. 13, no. 1, pp. 49–57, 1980.

[26] A. E. Minetti, C. Moia, G. S. Roi, D. Susta, and G. Ferretti, "Energy cost of walking and running at extreme uphill and downhill slopes," *Journal of applied physiology*, vol. 93, no. 3, pp. 1039–1046, 2002.

[27] R. D. Gregg, Y. Y. Dhaher, A. Degani, and K. M. Lynch, "On the mechanics of functional asymmetry in bipedal walking," *IEEE Trans. Biomedical Engineering*, vol. 59, no. 5, pp. 1310–1318, 2012.

[28] P. De Leva, "Adjustments to zatsiorsky-seluyanov's segment inertia parameters," *J. Biomechanics*, vol. 29, no. 9, pp. 1223–1230, 1996.

[29] R. E. Kelley and A. P. Borazanci, "Stroke rehabilitation," *Neurological research*, vol. 31, no. 8, pp. 832–840, 2009.